Composition Fluctuation Effects on Dielectric Normal-Mode Relaxation in Diblock Copolymers. 1. Weak Segregation Regime

K. Karatasos, S. H. Anastasiadis,*,† A. N. Semenov,‡ G. Fytas, M. Pitsikalis,§ and N. Hadjichristidis§

Foundation for Research and Technology—Hellas, Institute of Electronic Structure and Laser, P.O. Box 1527, 711 10 Heraklion, Crete, Greece

Received December 14, 1993; Revised Manuscript Received April 1, 1994•

ABSTRACT: Dielectric relaxation spectroscopy has been used to investigate the normal-mode relaxation in disordered diblock copolymer melts far from the order-to-disorder transition (ODT). The dielectric spectra are analyzed in order to quantitatively obtain the distribution of relaxation times in the disordered diblocks. The width of the relaxation function shows significant broadening relative to the respective homopolymer distributions when the temperature is decreased and/or the molecular weight is increased. The broadening is attributed to composition fluctuation effects on the normal-mode relaxation. These effects are theoretically accounted for by considering both the short-range fluctuations due to chain connectivity and the long-range concentration fluctuations in diblock copolymers due to the proximity to the ODT and their coupling to the individual block segmental dynamics. Theory not only captures the relative features of the distributions but also quantitatively compares very well with the experimental dielectric spectra.

I. Introduction

Diblock copolymers, consisting of a contiguous linear sequence of polymerized monomers of chemical species A (the A block) covalently bonded to a second contiguous linear sequence of monomers of a different chemical species B, represent an interesting class of polymeric materials with a rich variety of phase behavior.[1] The equilibrium phase morphologies of diblock copolymers are determined by the overall degree of polymerization, N, the overall volume fraction of, e.g., the A block, f, and the segment–segment Flory–Huggins interaction parameters, χ, which depends on temperature as $\chi = \alpha + b/T$ with $b > 0$. Since the entropic and enthalpic contributions to the free energy density scale as N^{-1} and χ, respectively, it is the product χN that dictates the equilibrium phase morphology for a certain composition f. For $\chi N < 10$, the equilibrium morphology is a melt with uniform composition (homogeneous or disordered state). However, the unfavorable interactions between the A and B blocks lead to a local segregation of dissimilar monomers, i.e., composition fluctuations. The connectivity between the two blocks thus leads to a correlation hole[1,2] corresponding to a fluctuation length scale of $O(R_g)$, with $R_g = (N/6)^{1/2}b$ being the copolymer radius of gyration and b the statistical segment length. As χN increases to $O(10)$, a delicate balance between entropic and enthalpic factors leads to an order–disorder transition (ODT) toward a microphase characterized by long-range order in its composition with a characteristic size on the order of the size of the molecules. At $\chi N \gg O(10)$, the domination of enthalpic terms leads to highly organized periodic domain microstructures.[3]

In a seminal theoretical work, Leibler[2] constructed a Landau expansion of the free energy to fourth order in a compositional order parameter field, $\psi(\mathbf{r}) = \varphi_A(\mathbf{r}) - f$, where $\varphi_A(\mathbf{r})$ is the microscopic volume fraction of A monomers at position $\mathbf{r}$, and he was able to map out the phase diagram of a diblock copolymer near the ODT in the parameter space χN vs f. Leibler also provided an expression for the disordered phase structure factor, $S(\mathbf{q}) = \langle \psi_q \psi_{-q} \rangle$, with ψ_q being the Fourier transform of $\psi(\mathbf{r})$, as

$$S(\mathbf{q}) = N/[F(x,f) - 2\chi N] \tag{1}$$

where $F(x,f)$ is related[2] to certain Debye correlation functions of a Gaussian block copolymer

$$g_D(f,x) = 2\,[fx + e^{-fx} - 1]/x^2 \tag{2}$$

with $x = q^2R_g^2$; this expression predicts a Lorentzian peak at $x = x^*(f) \approx [3/f(1-f)]^{1/2}$, with the peak intensity diverging at the stability limit, $F(x^*,f) - 2(\chi N)_s = 0$. The proximity to the transition point is usually expressed by $\epsilon = 2N(\chi_s - \chi)$. Fredrickson and co-workers[5] incorporated fluctuation corrections in the effective Hamiltonian for a diblock melt and found that the fluctuation corrections, controlled by a Ginsburg parameter, $\bar{N}$, defined[5,6] by $\bar{N} = Nb^6v^{-2}$, where v is the average segmental volume, lead to a suppression of the symmetric critical mean-field point that is replaced by a weak first-order transition at a lower temperature. In the Hartree approximation,[5] the structure factor $S(q)$ for a monodisperse diblock is modified from Leibler's mean-field result to be given by eq 1 by replacing χ with an effective interaction parameter, χ_{eff}, which depends on temperature, molecular weight, and composition and is related to the bare parameter.[5] The peak intensity does not diverge at the ODT, but it attains a maximum that is $O(N\bar{N}^{1/3})$ at a temperature lower than the mean-field stability limit.[5]

In contrast to the numerous experimental and theoretical investigations on the diblock copolymer morphology, the copolymer equilibrium dynamics only recently has attracted the interest of the scientific community.[7] Rheological measurements on disordered diblock copolymers[8] have shown evidence of substantial fluctuation enhancement of the shear viscosity and first normal stress coefficients, whereas the composition fluctuations near the ordering transition lead to a significant departure from thermorheological simplicity at low frequencies even for temperatures much higher than the ODT. Dielectric relaxation spectroscopy (DS)[8-14] and the photon correlation spectroscopy (PCS) techniques of dynamic light scattering in both the depolarized[12,15-19] and the polarized[17,20-22]

* Author to whom correspondence should be addressed.
† Also at Physics Department, University of Crete, 711 10 Heraklion, Crete, Greece.
‡ Permanent address: Physics Department, Moscow State University, 117234 Moscow, Russia.
§ Also at Chemistry Department, University of Athens, 157 01 Zografou, Athens, Greece.
• Abstract published in *Advance ACS Abstracts*, May 15, 1994.

0024-9297/94/2227-3543$04.50/0

Table 1. Molecular Characteristics of the Samples

sample	w_S[a]	f_S	M_n	M_w/M_n	N	T_g	$T_{g,PS}$[b]	T_s
SI-60	0.58	0.55	4450	1.07	57[c]	265	340	145
SI-100	0.62	0.59	7600	1.03	92[c]	278	353	195
SI-110	0.62	0.59	9100	1.03	110[c]	268	357	235
PI	0.0	0.0	3850	1.04	55[d]	206		

[a] Weight fraction of polystyrene (S). [b] Calculated with $1/T_{g,PS} = 1/373 + 0.72/M_{PS}$ in K^{-1} from ref 27. [c] Based on the average segmental volume. [d] Based on the PI segmental volume.

geometry have been utilized to investigate the segmental[8,12,15,16] and chain[9-11,13,14] dynamics, the relaxation of the concentration fluctuations in both disordered[17,20-23] and ordered[22] diblocks, and the orientation correlations in the disordered[19] and ordered[18] states. Moreover, forced Rayleigh scattering has been used to investigate the translational diffusion in homogeneous[23] and heterogeneous[24] diblocks and pulsed-field-gradient nuclear magnetic resonance to study the self-diffusion coefficient of copolymer chains.[21,23]

DS and PCS have provided clear evidence of the existence of two distinctly different segmental orientation times in homogeneous diblock copolymer melts, which proves the presence of two different local environments in diblocks, i.e., strong composition fluctuations even far above the ODT. The root-mean-square amplitude of these composition fluctuations estimated from the local segmental orientation times shows a significant increase with the proximity to the ODT.[25] An important characteristic of the segmental relaxation spectrum is the significant broadening[15] relative to the spectra of the parent homopolymers attributed to the heterogeneities in the system, due to the composition fluctuations, on the length scale of the characteristic length of the glass transition, ξ_α. The block end-to-end relaxation has been investigated using DS[9-14,25] and utilizing a polyisoprene (PI) block, that is a typical type-A polymer in the classification of Stockmayer,[26] i.e., it possesses a dipole moment component along the chain contour. For ordered diblocks, retardation and broadening of the PI normal mode were observed and attributed to both a spatial and a thermodynamic confinement of the PI blocks in the PI microdomains.[10] For disordered diblocks, the observed[13] broadening of the PI normal mode was significantly less than that for the segmental relaxation, since the end-to-end vector orientation effectively averages fluctuations over a much larger scale than ξ_α. Moreover, the relaxation time of the process could be accounted for by an effective friction almost equal to the average of the two blocks,[25] in contrast to the segmental times that require two local frictions different from the average.[25]

In this paper, we apply DS to experimentally and theoretically quantify the normal-mode relaxation behavior in symmetric disordered poly(styrene-*b*-1,4-isoprene) diblock copolymer melts far from the order-to-disorder transition. The distributions of relaxation times for the disordered diblocks are quantitatively obtained by analyzing the dielectric spectra using a modified inversion fitting procedure (section III). It is shown that the widths of the relaxation functions show systematic broadening relative to the respective homopolymer distributions when the temperature is decreased and/or the molecular weight is increased. The broadening is due to composition fluctuation and proximity to the glass transition effects on the normal-mode relaxation. These effects are theoretically accounted for (section IV) by a new approach that considers both the short-range fluctuations due to chain connectivity, that exist even in homopolymers and are independent of the block/block interactions, and the long-range composition fluctuations in diblock copolymers due to the proximity to the ODT. Theory not only captures the relative features of the distributions but also quantitatively compares very well with the experimental dielectric spectra, as discussed in section V.

II. Experimental Section

Materials. The poly(styrene-*b*-1,4-isoprene) (SI) diblocks were anionically polymerized under high vacuum in a glass-sealed apparatus at room temperature using benzene as the solvent and *sec*-BuLi as the initiator, with styrene being polymerized first. After completion of the reaction for both blocks, the living ends were neutralized with degassed t-BuOH. The number-average molecular weights of both the polystyrene (PS) blocks and the diblocks were determined by vapor pressure osmometry, whereas the mole fraction of PS was determined by ^1H NMR and the molecular weight distribution by gel permeation chromatography. The synthetic procedure produced a polyisoprene (PI) sequence with cis:trans:vinyl $\approx$ 72:20:8. The molecular characteristics of both copolymers are given in Table 1. The equilibrium phase morphology of the diblocks in the temperature range investigated is the homogeneous or disordered state, since the theoretical stability limit based on Leibler's theory[2] with literature interaction parameter data[18] is at much lower temperatures (Table 1). Homopolymer 1,4-polyisoprene (PI) was anionically synthesized under high vacuum and characterized by the standard techniques; its characteristics are also shown in Table 1.

DS. Dielectric relaxation spectroscopy was used to investigate the collective chain dynamics of the SI copolymers as a function of temperature. This is dielectrically observable due to the finite dipole moment component parallel to the chain contour of the PI sequence. The complex dielectric permittivity $\epsilon^*(\omega) = \epsilon'(\omega) - i\epsilon''(\omega)$ of a macroscopic system is given by the one-sided Fourier transform of the time derivative of the normalized response function[28] $C(t)$

$$\epsilon^*(\omega) - \epsilon_\infty = -\Delta\epsilon \int_0^\infty \frac{dC(t)}{dt} e^{-i\omega t}\, dt \tag{3}$$

where $i^2 = -1$, $\Delta\epsilon = \epsilon_0 - \epsilon_\infty$ is the relaxation strength, with ϵ_0 and ϵ_∞ being the low- and high-frequency limiting values of ϵ'. The quantity $C(t)$ is the normalized dipole autocorrelation function

$$C(t) = \sum_{jk} \langle \mu_j(t)\, \mu_k(0) \rangle / \sum_{jk} \langle \mu_j(0)\, \mu_k(0) \rangle \tag{4}$$

where $\mu_j(t)$ is the dipole moment of jth segment at time t. For nonzero dipole moment components $\mu^\parallel$ and $\mu^\perp$ parallel and perpendicular to the chain contour, respectively, the response function $C(t)$ can be decomposed into contributions of segmental and overall chain orientations. Neglecting cross correlations between segments of different chains, the autocorrelation function $C(t)$ for the ith chain can be written as[29]

$$C(t) \propto \sum_{jk} \langle \mu_{ij}^\perp(t)\, \mu_{ik}^\perp(0) \rangle + \sum_{jk} \langle \mu_{ij}^\parallel(t)\, \mu_{ik}^\parallel(0) \rangle \tag{5}$$

The first correlation function, $C^\perp(t)$, is sensitive to segmental motion, whereas the second function, $C^\parallel(t)$, represents the end-to-end vector correlation function

$$C^\parallel(t) = (\mu^\parallel)^2 \langle \mathbf{R}_i(t)\, \mathbf{R}_i(0) \rangle \tag{6}$$

where $\mathbf{R}_i(t)$ is the end-to-end vector of the ith subchain. The

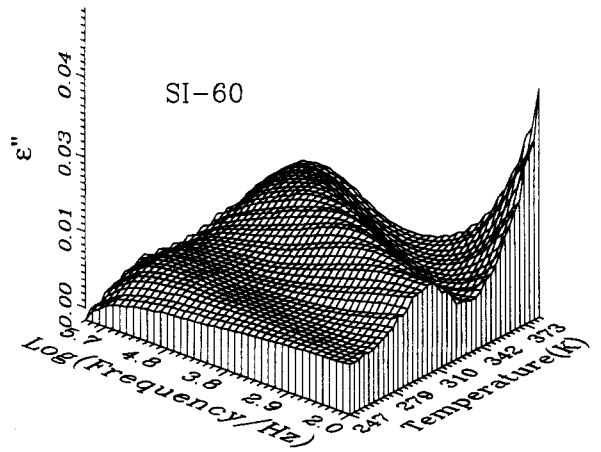

Figure 1. Temperature and frequency dependence of the dielectric loss ϵ'' for the SI-60 diblock copolymer in the homogeneous state. The segmental and the normal-mode relaxations of the PI subchain are clearly observed at high and low frequencies, respectively.

strength $\Delta\epsilon_n$ associated with the dielectric normal-mode relaxation (eq 6) is given by

$$\Delta\epsilon_n = \frac{N_A(\mu^{\parallel})^2\langle R^2\rangle\rho}{3M_n k_B T}F \tag{7}$$

where N_A is Avogadro's number, ρ the mass density, M_n the number-average molecular weight of the polymer, k_B Boltzmann's constant, T the temperature, and F the internal field factor, which for normal-mode relaxation is taken to be unity.[30]

The dielectric measurements were performed using a Hewlett-Packard HP 4284 A impedance analyzer based on the principle of the ac bridge technique in the frequency range 20–10^6 Hz. The sample was residing between two gold-plated stainless steel electrodes (diameter 25 mm) with a spacing of 50 ± 1 μm maintained by two fused silica fibers 50 μm in diameter. The sample was kept in a cryostat with its temperature controlled by the Novocontrol Quatro system controller via a high-pressure nitrogen gas jet heating system allowing a stability of the sample temperature in margins of ±0.1 °C in a broad temperature range of −160 to +300 °C. The typical resolution in tan $\delta = \epsilon''/\epsilon'$ is quoted to be $<10^{-4}$.

For quantitative analysis, the generalized relaxation function according to Havriliak–Negami[31] (HN) is traditionally being used

$$\epsilon^*(\omega) = \epsilon_\infty + \frac{\epsilon_0 - \epsilon_\infty}{[1 + (i\omega\tau)^\alpha]^\gamma} \tag{8}$$

where α and γ are parameters ($0 \le \alpha, \gamma \le 1$) describing the symmetric and asymmetric broadening of the relaxation time distribution (in log ω scale), respectively. The case $\alpha = \gamma = 1$ corresponds to a simple exponential decay of $C(t)$. An additional conductivity contribution at low frequencies and high temperatures due to free charges is accounted for by the power law dependence

$$\epsilon''(\omega) = \sigma_0/\epsilon_v\omega^s \tag{9}$$

where σ_0 and s are fit parameters ($0 \le s \le 1$) and ϵ_v denotes the permittivity in free space.

III. Data Analysis and Results

III.a. Dielectric Relaxation Spectra. Figure 1 shows a three-dimensional representation of the loss part of the dielectric permittivity, $\epsilon''(\omega)$, for the homogeneous diblock copolymer SI-60 in the frequency range 20–10^6 Hz and for temperatures 245–375 K. The dielectric spectra resemble typical spectra of PI homopolymers[29] and show two distinct relaxation processes, well separated in the frequency–temperature space, and the conductivity contribution at low frequencies and high temperatures. The high-frequency and low-temperature relaxation displays a

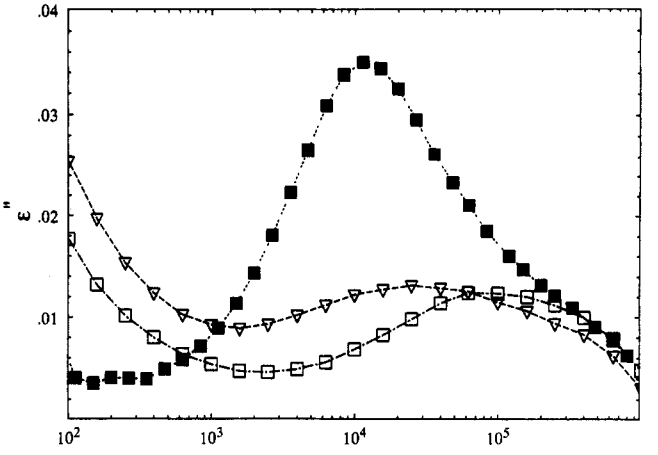

Figure 2. Dielectric loss $\epsilon''(\omega)$ for homopolymer PI at 295 K (■) and disordered diblock copolymers SI-60 (□) and SI-100 (▽) at 365 K. The relaxation processes are assigned to the normal mode of PI blocks.

stronger temperature dependence and has been attributed to the segmental relaxation in PI-rich microenvironments of the disordered diblocks.[13] It has been shown before that the segmental relaxation exhibits a much broader distribution of relaxation times when compared to the segmental relaxation of pure homopolymer PI[13,15,25] due to composition fluctuation effects on the length scale ξ_α, associated with the glass transition. The low-frequency and high-temperature relaxation has been attributed to the PI-block end-to-end orientation, i.e., to the PI-block normal-mode relaxation in the disordered state.[13,14,25] The distribution of relaxation times for the normal-mode process is narrower than that for the segmental process but still broader than the one for PI homopolymers of comparable chain length, as will be discussed later. The two processes exhibit apparently different temperature dependencies, similarly to the behavior for pure PI homopolymers.[13,14,25,28]

Figure 2 shows a comparison of the dielectric loss data for the normal-mode relaxation processes between a PI homopolymer at 295 K and the two disordered diblock copolymers SI-60 and SI-100 at 365 K. Comparison with PI at different temperatures is meaningful, since it has been shown that the distribution of relaxation times for PI homopolymer is essentially insensitive to temperature;[29] it does, however, depend on the molecular weight, as will be discussed later. The data in Figure 2 clearly show a significant increase in the width of the dielectric loss curve between the homopolymer and each one of the two diblocks, to be quantified later. Similarly, the relaxation spectra get broader as the molecular weight of the copolymer is increased between the SI-60 and the SI-100 diblocks. Two reasons may be responsible for the excess broadening: the relative increase of the composition fluctuation effects going from the homopolymer PI to SI-60 and SI-100 and the increased proximity to the calculated average glass transition temperature, T_g, in the same sequence (Table 1). Both these effects will be quantitatively considered in section IV.

The effect of temperature on the broadening of the experimental dielectric spectra is illustrated in Figure 3, displaying experimental $\epsilon''(\omega)$ for SI-60 at 325 and 345 K. The width of the dielectric spectra is shown to increase significantly as the temperature is decreased. The conventional analysis of the dielectric loss data employing the HN fit (eq 8) together with the conductivity contribution (eq 9) is shown in Figure 3 to describe the data within experimental accuracy. For the record, the fitting pa-

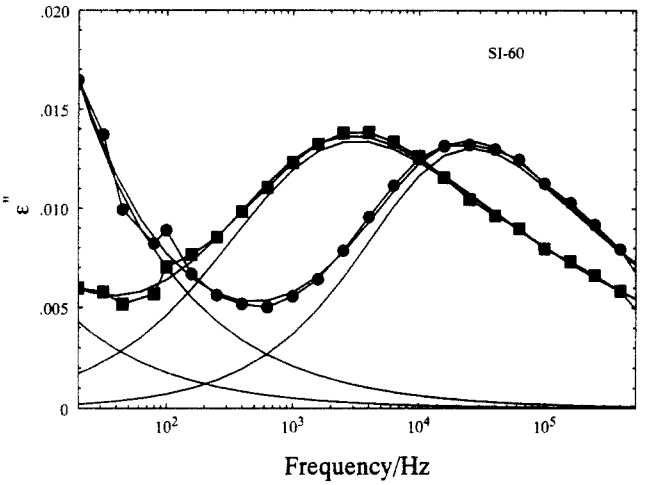

Figure 3. Dielectric loss $\epsilon''(\omega)$ for the PI-subchain normal-mode relaxation at 325 (■) and 345 K (●) for the disordered SI-60. The solid lines correspond to the conventional analysis of the data using a Havriliak–Negami function for the relaxation process (eq 8) and a conductivity contribution (eq 9).

rameters required to account for the data are $\Delta\epsilon = 0.072$, $\alpha = 0.68$, $\gamma = 0.36$, $\sigma_0 = 5.2 \times 10^{-15}$ $(\Omega\ \mathrm{cm})^{-1}$, $s = 0.55$ at 325 K and $\Delta\epsilon = 0.056$, $\alpha = 0.75$, $\gamma = 0.44$, $\sigma_0 = 1.8 \times 10^{-14}$ $(\Omega\ \mathrm{cm})^{-1}$, $s = 0.52$ at 345 K, in qualitative agreement with previous investigations[13] and in agreement with the observation that the width increased as the temperature is decreased. The behavior for the higher molecular weight diblocks SI-100 and SI-110 is qualitatively the same, i.e., the width of $\epsilon''(\omega)$ increases with decreasing temperature. Quantitative comparison of the distribution functions for the normal-mode relaxation will be presented later in connection to Figure 7. In the next subsection, a method is presented to quantitatively extract the distributions of relaxation times from dielectric data without an a priori assumption for the form of the relaxation function, e.g., eq 8, but only assuming a superposition of exponentials.

III.b. Distribution of Relaxation Times. The traditional analysis of dielectric spectra using the well-known HN function (eq 8) provides, in most cases, a satisfactory description of the experimental spectra; the absence, however, of a clear physical interpretation of the adjustable parameters involved and the fitting uncertainties restrict the use of eq 8 solely as a phenomenological way to account for the features of the underlying processes. A direct transformation of the dielectric data in order to obtain the distribution of relaxation times with no a priori assumption of the form of the relaxation function is certainly more appropriate. We present here a way to extract the distribution of relaxation times directly from dielectric loss data.

For a single Debye process, i.e., a single relaxation time, τ, eq 3 becomes

$$\frac{\epsilon^*(\omega) - \epsilon_\infty}{\Delta\epsilon} = \frac{1}{1 + i\omega\tau} \tag{10}$$

In order to describe the usual nonexponential behavior of real polymer systems, a superposition of Debye processes is employed that implies a spectrum of retardation times, i.e.,

$$\frac{\epsilon''(\omega)}{\Delta\epsilon} = \sum_i g_i \frac{\omega\tau}{1 + (\omega\tau)^2} \tag{11a}$$

with g_i being the appropriate weighting factor, which in the continuous limit leads to

$$\frac{\epsilon''(\omega)}{\Delta\epsilon} = \int_0^\infty G(\tau) \frac{\omega\tau}{1 + (\omega\tau)^2}\, d\tau \tag{11b}$$

with $G(\tau)$ the distribution of relaxation times. It is more convenient to utilize a logarithmic time scale, in which case

$$\frac{\epsilon''(\omega)}{\Delta\epsilon} = \int_{-\infty}^\infty F(\ln\tau) \frac{\omega\tau}{1 + (\omega\tau)^2}\, d(\ln\tau) \tag{12}$$

where both forms of the distribution are assumed to be normalized and $F(\ln\tau) = \tau G(\tau)$.

Various methods have been proposed in the literature in order to calculate $G(\tau)$ or, equivalently $F(\ln\tau)$, most recently the histogram[32] and the deconvolution method based on Fourier transforms.[33] Although valuable information can, in principle, be extracted, several ambiguities are present in both methods. In the histogram method, the problems are associated mainly with the sensitivity to small experimental errors in $\epsilon''(\omega)$ that may create artifacts, as well as the fact that the resulting distribution is not smooth, with the resulting peaks and valleys leading to possible erroneous conclusions. Besides the usual problems associated with Fourier transforms, which not always can be efficiently overcome, the deconvolution method provides no complementary information related to the acceptance of the proposed solution on physical grounds.

The method proposed here is basically a modified version of the widely used CONTIN routine[34] of analysis of photon correlation spectroscopy data[35] based on an inverse Laplace transform (ILT) of the experimental correlation function. A significant advantage of this routine is that it provides reliable statistical criteria for the support or rejection of the nominal proposed solutions. CONTIN performs an inversion of the experimental relaxation function, $C(x)$, in order to determine the distribution $F(\ln\tau)$, of the general form

$$C(x) = \int K(x,\tau)\, F(\ln\tau)\, d(\ln\tau) \tag{13}$$

where $K(x,\tau)$ represents the kernel of the transform. Direct comparison of eqs 12 and 13 dictates that for dielectric spectroscopy

$$C(\omega) = \frac{\epsilon''(\omega)}{\Delta\epsilon} \quad \text{and} \quad K(\omega,\tau) = \frac{\omega\tau}{1 + (\omega\tau)^2} \tag{14}$$

More conveniently, eq 13 may be written as

$$\epsilon''(\omega) = \int_{-\infty}^\infty \tilde{F}(\ln\tau) \frac{\omega\tau}{1 + (\omega\tau)^2}\, d(\ln\tau) \tag{15}$$

where $\tilde{F}(\ln\tau) = \Delta\epsilon F(\ln\tau)$; integration of the resulting $\tilde{F}(\ln\tau)$ spectrum yields $\Delta\epsilon$, since the $F(\ln\tau)$ distribution is normalized. In the course of this work, a similar procedure of inverting dielectric relaxation data has also been worked out by a different group.[36]

The accuracy and precision of the above-outlined method of analysis of dielectric loss data will be illustrated by analyzing simulated $\epsilon''(\omega)$ based on a known distribution and comparing the extracted distribution of relaxation times to the analytical expressions. Figure 4 shows simulated dielectric loss spectra based on eq 12, using a normalized bimodal $\tilde{F}(\ln\tau)$ of the form

$$\tilde{F}(\ln\tau) = \tau(a_1\delta(\tau - \tau_1) + a_2\delta(\tau - \tau_2)) \tag{16}$$

i.e., $G(\tau)$ is the sum of two delta functions at τ_1 and τ_2 differing by a factor of 10 and with amplitude ratios a_1:a_2 assuming the values of 1 (Figure 4a) and 5 (Figure 4b). The comparison between the distribution of relaxation

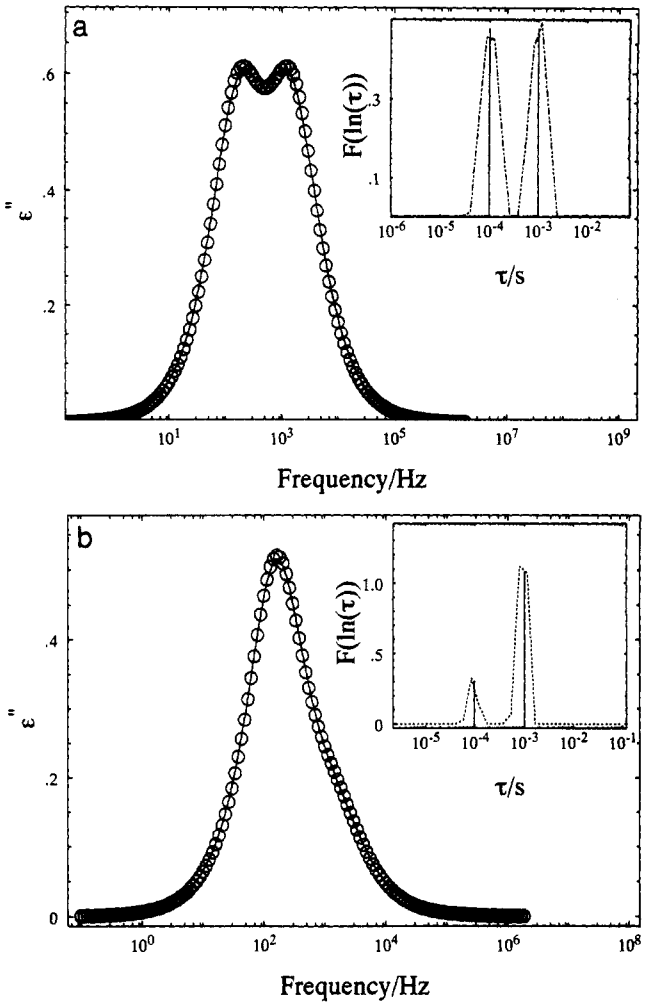

Figure 4. Simulated dielectric loss data and their quantitative analysis in order to obtain the distribution of relaxation times. The simulation for $\epsilon''(\omega)$ (O) uses eq 12 with the distribution of eq 16. The solid line represents the fit to the simulated data. The insets show comparisons of the distribution of relaxation times $F(\ln \tau)$ obtained according to the procedure outlined in section III (dotted line) with the distribution of eq 16 of two delta functions with $\tau_1 = 10^{-3}$ s, $\tau_2 = 10^{-4}$ s, and (a) $a_1:a_2 = 1:1$ or (b) $a_1:a_2 = 5:1$.

times obtained by the inversion procedure outlined above and the assumed distribution $F(\ln \tau)$ of eq 16 is shown in the inset of parts a and b of Figure 4, respectively. This figure illustrates the ability of the analysis method to extract both time and dielectric strength information with very good precision for double exponentials with relaxation times differing by 1 order of magnitude even when the ratio of their amplitudes differs by a factor of 5.

The applicability of the analysis procedure to real experimental data is illustrated in Figure 5 where the dielectric spectrum of a PI homopolymer at 294 K is analyzed. PI normal-mode relaxation has been shown[29] to be accurately described by HN functions (eq 8) with $\alpha = 1$ and $\gamma = 0.47$ which correspond to the well-known Cole–Davindson functions.[37] The distribution of relaxation times obtained by inversion of the dielectric loss data for homopolymer PI, shown in the inset of Figure 5, is compared with the calculated distribution based on an analytical expression for the distribution of relaxation times for the Cole–Davidson functions[38]

$$F(\ln \tau) = \begin{cases} \tau \dfrac{\sin(\pi\gamma_{CD})}{\pi}\left[\dfrac{\tau}{\tau_{CD}-\tau}\right]^{\gamma_{CD}} & \text{for } \tau < \tau_{CD} \\ 0 & \text{for } \tau \geq \tau_{CD} \end{cases} \quad (17)$$

The parameter γ_{CD} determines the width of the distribution and decreases with increasing width of the distribution of relaxation times. The main characteristics of the obtained distribution function are the asymmetric character of the distribution with a long tail at the short times side and, hence, high frequencies, and the pseudopeak at long times corresponding to the conductivity contribution at low frequencies in the experimental $\epsilon''(\omega)$ data. The analysis algorithm regards the increase in $\epsilon''(\omega)$ data as the frequency decreases with the initial rise of a relaxation process that is currently outside the experimental frequency window. This peak, however, does not interfere with the estimation of the normal-mode relaxation distribution function. It should be noted that the area under the peak of the distribution function is the dielectric strength $\Delta\epsilon$ of the process.

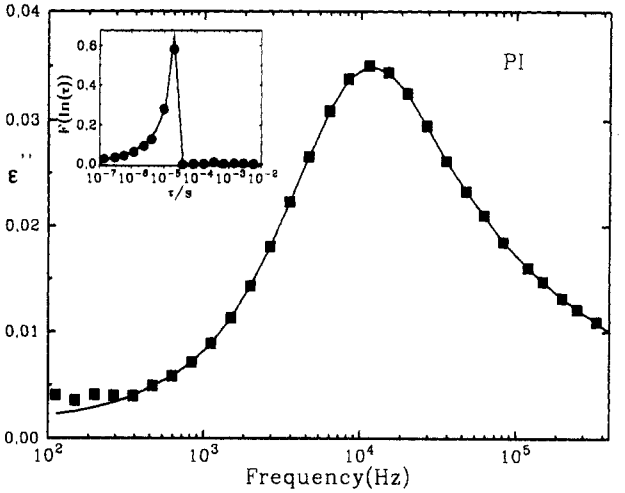

Figure 5. Dielectric loss $\epsilon''(\omega)$ for homopolymer PI at 295 K (■), with the calculated curve (solid line) based on the distribution of relaxation times $F(\ln \tau)$ obtained according to the procedure outlined in section III. In the inset the distribution of relaxation times (●) is compared to the analytical expression for $F(\ln \tau)$ according to eq 17 with $\gamma_{CD} = 0.47$.

Figure 6 shows the distribution functions obtained from the inversion of the experimental dielectric loss data for the diblock copolymers SI-60 (Figure 6a) and SI-100 (Figure 6b) for various temperatures. The increased broadening of the distribution as the temperature is decreased is now quantitatively evident, as is the asymmetric broadening of the distributions toward short times. The expected increase of $\Delta\epsilon$ with decreasing temperature (eq 7) is clearly evident in Figure 6a, whereas it is obscured in Figure 6b due to the high conductivity contribution. Figure 7 shows the temperature dependence of the characteristic relaxation times of the normal-mode process in an Arrhenius plot (Figure 7a) and of the full width at half-maximum (fwhm) of the distributions (Figure 7b). The relaxation times follow the well-known Vogel–Fulcher–Tamann–Hesse (VFTH) equation

$$\tau = \tau^\circ \exp\left[\frac{B}{T - T_0}\right] \quad (18a)$$

with parameters B, T_0, and τ° shown in Table 2. B is the activation parameter and T_0 the ideal glass transition temperature. For consistency, in the fits shown in Figure 7a the average calorimetric T_g of the diblocks was taken into account as well as the N^2 dependence of τ°. Figure 7b shows the dramatic dependence of the fwhm of the distributions of Figure 6 on temperature for the three diblocks compared to the fwhm for PI homopolymer that on the contrary is insensitive to temperature and much narrower. It should be noted that the fwhm for all three diblocks are very similar. This may lead us to believe that the main contribution to the width of the distribution is due to the presence of polystyrene segments in the

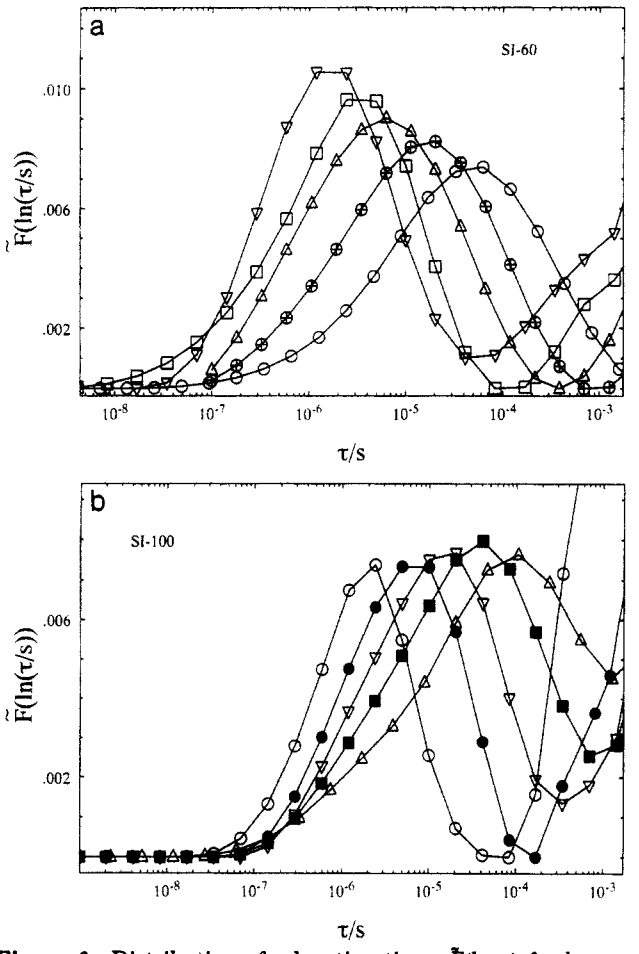

Figure 6. Distribution of relaxation times $\tilde{F}(\ln \tau)$ for homogeneous diblock copolymers at various temperatures obtained from the dielectric loss data according to the procedure outlined in section III: (a) SI-60 at (from left to right) 365, 355, 345, 335, and 325 K; (b) SI-100 at (from left to right) 385, 365, 355, 345, and 335 K.

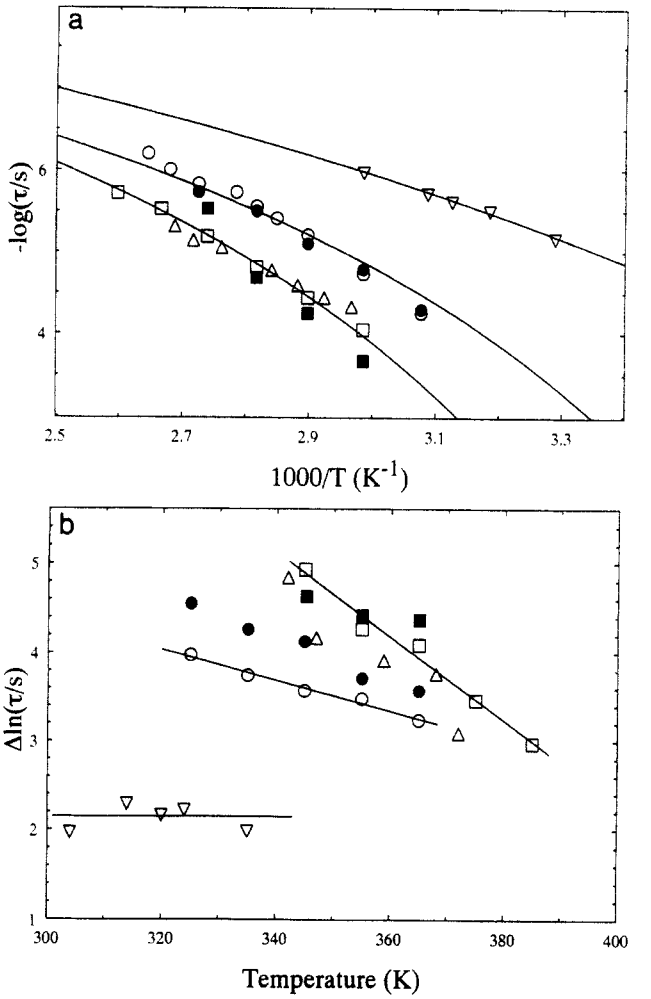

Figure 7. Temperature dependence of (a) the normal-mode relaxation times and (b) the full width at half-maximum of the distribution of relaxation times for (▽) homopolymer PI, (○) SI-60, (□) SI-100, and (△) SI-110. Theoretically calculated values (see section IV and V) are shown for SI-60 (●) and SI-100 (■). The solid lines in a are VFTH (eq 18) fits to the experimental relaxation times with the parameters in Table 2, whereas in b they guide the eyes.

proximity of the PI chains and not really to the amplitude of the composition fluctuations, which, for the same temperature, should depend on the molecular weights of the diblocks. One should remember, however, that the three diblocks are far from their ODT.

In the next section a theoretical approach will be presented in order to quantitatively account for the proximity both to the glass transition and to the amplitude of composition fluctuations in the disordered diblocks.

IV. Theoretical Approach

Dielectric relaxation spectroscopy essentially measures the time-correlation function of the end-to-end vector orientation of PI blocks. In what follows, we will consider disordered diblock copolymers with equal segmental volumes, v, and statistical segment lengths, b, and block sizes N_A and N_B, with A = PI specifying the dielectrically active block, type-A chain.

In the presence of composition fluctuations,[25] one would expect that conformational relaxation of the A = PI blocks should be faster than that for the B = PS blocks, since the glass transition temperature for the PS component is significantly higher than that for PI. Moreover, it has been documented that the segmental relaxation times in the PS-rich and PI-rich microenvironments in disordered diblocks differ by up to 6 orders of magnitude.[15,17,25] Therefore, in the following theoretical treatment, it will be assumed that the B blocks are nearly immobile during the relaxation of the A blocks, i.e., that the junction points are fixed during the process. This assumption will make the physical model described below more clear, whereas, on the other hand, it does not affect the final results.

Table 2. VFTH Parameters for the Normal-Mode Relaxation

sample	$-\log[\tau°/s]$	B_n (K)	$T_n°$ (K)
SI-60	9.24	1206	215
SI-100	9.57	1380	228
SI-110	9.84	1573	218
PI	9.76	1560	156

For nonentangled linear polymer chain A with one fixed end, the end-to-end vector correlation function is expressed by the Rouse free-draining model[26,39]

$$I(t) = \langle R_i(t)\, R_i(0)\rangle / \langle R^2\rangle = \frac{8}{\pi^2} \sum_{p=\text{odd}} \frac{1}{p^2} \exp\left(-\frac{p^2 t}{\tau_R}\right) \qquad (19)$$

with τ_R being the Rouse longest relaxation time, $\tau_R = (4\zeta b^2/3\pi^2 k_B T) N_A^2 \equiv \tau_0 N_A^2$, with τ_0 an effective local time determined by the local friction ζ. Taking into account only the longest relaxation time, i.e., neglecting any faster components due to their small amplitude which scales with $1/p^2$, the relaxation function may take the form $I(t) \cong \exp(-t/\tau_R)$. Since our aim is to predict the excess broadening observed in disordered diblock copolymers in comparison to homopolymers and the inherent homopolymer widths will be introduced later (eq 40), it is not so severe an approximation to use the Rouse model with the

above assumption in the theoretical calculation at this stage.

In the undiluted bulk state, the local time τ_0 depends strongly on temperature and has been shown to follow the VFTH equation (eq 18) with a different intercept and slightly different activation parameter and ideal glass transition temperature

$$\tau_0 = \tau_0^\circ \exp\left[\frac{B}{T - T_0}\right] \tag{18b}$$

where the subscript 0 denotes local jump relaxation times responsible for normal-mode relaxation. For a compatible mixture of two polymers with volume fractions $\varphi_A = \varphi$ and $\varphi_B = 1 - \varphi$, the free volume model[40] leads to the following mixing rules[14] for the parameters B and T_0:

$$\frac{1}{B} = \frac{\varphi}{B_A} + \frac{(1-\varphi)}{B_B}; \quad T_0 = \frac{\varphi T_{0,A} B_B + (1-\varphi) T_{0,B} B_A}{\varphi B_B + (1-\varphi) B_A} \tag{20}$$

Equations 18b and 20 show a strong dependence of the local jump time on local composition. For small deviations from the average composition, a Taylor expansion around the average volume fraction of B,φ, results in

$$\ln \tau_0(\varphi) = \ln \tau_0(\tilde{\varphi}) + C\Delta\varphi \tag{21}$$

where $\ln \tau_0(\tilde{\varphi})$ is calculated from eq 18b and $C = \partial/\partial\varphi\,(B(\varphi)/[T - T_0(\varphi)])|_{\varphi=\tilde{\varphi}}$, which both depend on the average composition. $\Delta\varphi = \varphi - \tilde{\varphi}$ is the increment in the volume fraction of B, e.g., for our case PS. Therefore, composition fluctuations lead to a fluctuation in the effective local time τ_0 that results in a broadening of the relaxation spectra. Two origins of composition fluctuations should be considered in the case of diblock copolymer melts: (a) the short-range fluctuations due to chain connectivity, that are always present and essentially independent of the interaction parameter, χ, and are almost the same for copolymers and blends; (b) the long-range fluctuations, with wavelength on the order of the size of the copolymers ($\propto N^{1/2}b/\sqrt{6}$), that are characteristic of diblock copolymer thermodynamics and their amplitudes increase with the proximity to the ODT.

Let n be the position of a PI link along the chain with $n = 0$ corresponding to the free end. The end-to-end vector orientation correlation may be alternatively defined via the relaxation of the block dipole moment after one has switched off a weak orientational field at $t = 0$. Therefore, $I(t)$ may be represented as a sum of contributions of all links ($n = 0, 1, ..., N_A$):

$$I(t) = \frac{1}{N_A}\sum_{n=0}^{N_A} I_n(t) \tag{22a}$$

where $I_n(t)$ relates to the mean dipole moment of the nth link. Relaxation of this dipole moment may be approximately described by Rouse dynamics for the subchain consisting of n links:

$$I_n(t) \cong \exp[-t/(\tau_0 n^2)] \tag{23}$$

Thus, the relaxation is considered to start at the free PI end and to proceed down to the junction point, which is assumed to be fixed. In the general case, τ_0 is the average local jump time in the volume spanned by the n-segment subchain that is determined by the average composition, $\hat{\varphi} \equiv \hat{\varphi}_{PS}$; fluctuations of this $\hat{\varphi}$ are slow as they are determined by the dynamics of the PS block on a length scale on the order of the block size and n is typically on the order of $N_A \cong N/2$. Thus, one may assume that during the PI normal-mode relaxation $\hat{\varphi}$ is constant; therefore, it is the distribution in $\hat{\varphi}$ that leads to a distribution in the relaxation times, $\tau_{Rn} \equiv \tau_0(\hat{\varphi})\, n^2$. Note that, without composition fluctuations, eqs 22a and 23 can be represented as

$$I(t) = \int_1^\infty \frac{1}{p^2} \exp\left(-\frac{p^2 t}{\tau_R}\right) dp \tag{22b}$$

which is similar to eq 19, and the difference is only due to the approximate nature of eq 23. The difference between eqs 19 and 22b is not important, since it is almost completely masked by composition fluctuations.

Let's define the distribution of relaxation times $\mu(\ln \tau)$, such that

$$I(t) = \int \mu(\ln \tau)\, e^{-t/\tau}\, d(\ln \tau) \tag{24}$$

Using eqs 23 and 24, one gets

$$\mu(\ln \tau) = \frac{1}{N_A}\int_0^{N_A} \mu_n(\ln \tau)\, dn \tag{25}$$

$$\mu_n(\ln \tau) = \tilde{\mu}_n(\ln \tau - 2 \ln n) = \tilde{\mu}_n(\ln \tau_0) \tag{26}$$

since the Rouse time $\propto n^2$. If one neglects the presence of composition fluctuations, $\tilde{\mu}_n(\ln \tau_0) = \delta(\ln \tau_0 - \ln \tau_0(\tilde{\varphi}))$. Let $P_n(\Delta\hat{\varphi})$ be the probability density for the composition fluctuation averaged over the n-segment subchain. Then, use of eq 21 results in

$$\tilde{\mu}_n(\ln \tau_0) = \frac{1}{C} P_n(\Delta\hat{\varphi}) = \frac{1}{C} P_n\left(\frac{\ln \tau_0 - \ln \tau_0(\tilde{\varphi})}{C}\right) = \frac{1}{C} P_n\left(\frac{\ln \tau - 2 \ln n - \ln \tau_0(\tilde{\varphi})}{C}\right) \tag{27}$$

Therefore, one should calculate $P_n(\Delta\hat{\varphi})$.

The distribution P_n is assumed to be Gaussian[5,6]

$$P_n(\Delta\hat{\varphi}) = \frac{1}{(2\pi\sigma_n^2)^{1/2}} \exp\left[-\frac{(\Delta\hat{\varphi})^2}{2\sigma_n^2}\right] \tag{28}$$

$\sigma_n^2 = \langle(\Delta\hat{\varphi})^2\rangle|_n$ is the variance of the Gaussian distribution, where $\Delta\hat{\varphi} = 1/n\sum_{i=1}^n \delta\varphi(\mathbf{r}_i)$, with $\delta\varphi(\mathbf{r})$ being the local composition fluctuation at point $\mathbf{r}$ and $\mathbf{r}_i$ being the current position of the ith link. Assuming that the fluctuation $\delta\varphi(\mathbf{r})$, which is determined by the overall distribution of polymer links, is virtually independent of the conformation of a given chain, we may write

$$\sigma_n^2 = \sum_{i,j=1}^{n} \langle S(\mathbf{r}_i - \mathbf{r}_j)\rangle \tag{29a}$$

where $S(\mathbf{r}) = \langle \delta\varphi(0)\, \delta\varphi(\mathbf{r})\rangle$ is the ordinary composition fluctuation function in real space. Thus

$$\sigma_n^2 = \int S(\mathbf{r})\, g_n(\mathbf{r})\, d^3r \tag{29b}$$

where $g_n(\mathbf{r})$ is the autocorrelation function for the links of an n-segment subchain

$$g_n(\mathbf{r}) = \frac{1}{n^2}\sum_{i,j=1}^{n} \langle \delta(\mathbf{r}_i - \mathbf{r}_j - \mathbf{r})\rangle; \quad \int g_n(\mathbf{r})\, d^3r = 1 \tag{30}$$

Introducing the Fourier representation of $S(\mathbf{r})$ and $g_n(\mathbf{r})$, $S(\mathbf{r}) = \int S(\mathbf{q}) \exp[i\mathbf{q}\cdot\mathbf{r}]\, d^3q/(2\pi)^3$ and $g_n(\mathbf{r}) = \int g_n(\mathbf{q}') \exp[i\mathbf{q}'\cdot\mathbf{r}]\, d^3q'/(2\pi)^3$, in the wavevector q space, eq 29b can also be written as

$$\sigma_n^2 = \int S(\mathbf{q})\, g_n(-\mathbf{q})\, d^3q/(2\pi)^3 \tag{31}$$

In this representation, $g_n(\mathbf{q})$ is the Debye function (eq 2) with $g_n(\mathbf{q}) = g_D(1, nb^2q^2/6)$ and $S(\mathbf{q})$ is the static structure factor given by eq 1.

Therefore, using eqs 26–28 one may calculate the distribution function as

$$\mu(\ln\tau) = \frac{1}{N_A}\int_0^{N_A} 1 \frac{1}{C}\frac{1}{(2\pi\sigma_n^2)^{1/2}} \times \exp\left[-\frac{(\ln\tau - 2\ln n - \ln\tau_0(\tilde{\varphi}))^2}{2C^2\sigma_n^2}\right] dn \quad (32)$$

with σ_n given by eq 31 and C by eq 21 based on homopolymer activation parameters B and ideal glass transitions T_0. In the calculations, we have used the B and T_0 parameters of the normal-mode process for PI homopolymer[13,29] and of the segmental mode for PS.[13] It should also be noted that in the following the distribution function of eq 32 is always normalized.

For a symmetric diblock ($N_A = N_B = N/2$) near the ODT, the function $F(x,f)$ becomes

$$F(x,f=0.5) = 4/[g_D(1,x/2) - g_D(1,x)] \quad (33)$$

with $x = Nb^2q^2/6$. Near the ODT ($|\chi - \chi_s| < \chi_s$) and for x near the position of the maximum of the structure factor at x^*, $x^*(f=0.5) \cong 3.8$, $F(x,0.5)$ may be approximated as $F(x^*+\Delta x,f=0.5) = 21 + 0.48(\Delta x)^2$, whereas $F(x^*,f=0.5) = 21$. Therefore, in this regime, the structure factor of eq 1 becomes

$$S(\mathbf{q}) \cong \frac{N}{2}\frac{1}{\epsilon_t + 0.24(\Delta x)^2} \quad (34)$$

with $\epsilon_t = (\chi_s - \chi)N$. Using eqs 33 and 34 in eq 31, one may approximately get

$$\sigma_n^2 = \Gamma g_D\left(\frac{n}{N}x^*\right) \quad (35)$$

where

$$\Gamma = \left(\frac{x^*}{0.24}\right)^{1/2}\frac{1}{8\pi}\frac{6^{3/2}v}{b^3}\frac{1}{N^{1/2}}\frac{1}{\epsilon_t^{1/2}} \cong 2.33\frac{v}{b^3}\frac{1}{N^{1/2}}\frac{1}{\epsilon_t^{1/2}} \quad (36)$$

leading to

$$\mu_{sym}(\tau) = \int_0^1 C\frac{1}{(2\pi)^{1/2}}\frac{1}{\sqrt{\Gamma}}\frac{1}{[g_D(zx^*/2)]^{1/2}} \times \exp\left[-\frac{(\ln\tau - 2\ln n - \ln\tau_0(\tilde{\varphi}))^2}{2C^2\Gamma g_D(zx^*/2)}\right] dz \quad (37)$$

Note that the width of the relaxation spectrum, $\Delta(\ln\tau)$ predicted by eq 37 is

$$\Delta(\ln\tau) \propto C\Gamma^{1/2} \propto C\frac{(v/b^3)^{1/2}}{N^{1/4}\epsilon_t^{1/4}} \quad (38)$$

In the mean-field model of Leibler,[2] the parameter $\epsilon_t = \chi_s - \chi$ decreases down to zero at the stability limit; therefore, the width $\Delta(\ln\tau)$ would tend to infinity as $\chi \to \chi_s$. However, fluctuation corrections[5] limit the increase of $\Delta(\ln\tau)$; the maximum width will be

$$[\Delta(\ln\tau)]_{max} \propto C\bar{N}^{-1/6} \quad (39)$$

where $\bar{N}$ is the Ginsburg parameter, where it was taken into account that, with the fluctuation corrections, the minimum value of the effective parameter ϵ_t is on the order[5] of $\bar{N}^{-1/3}$.

V. Discussion

Figure 8 shows the theoretical distribution of relaxation times, $\mu(\ln\tau)$, for various temperatures obtained using eqs 31 and 32 for the homogeneous diblock copolymer SI-60 with the molecular characteristics given in Table 1.

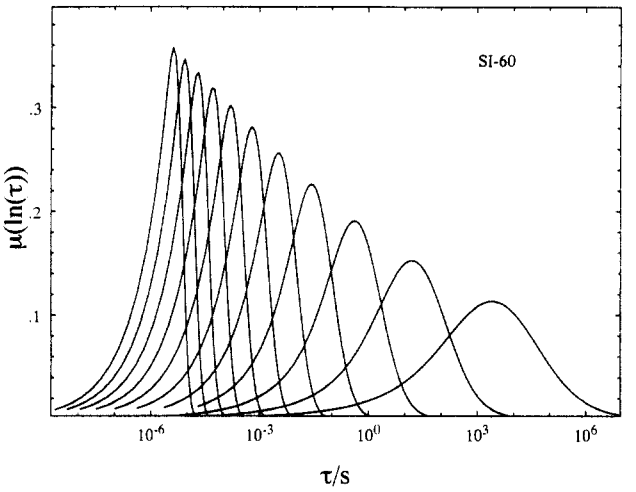

Figure 8. Calculated distributions of relaxation times for various temperatures (from left to right, 365–265 K every 10 K) for copolymer SI-60 based on the theoretical approach of section IV. The distributions do not include the inherent distributions of homopolymer PI.

The more simple eqs 36–39 cannot be used here, since in our experiments the diblocks were not close enough to the ODT. The structure factor $S(\mathbf{q})$ is calculated[2] using eq 1 with literature interaction parameter values,[18] $\chi = -0.05 + 34/T$, based on the average segmental volume. The distribution functions show the expected broadening as the temperature decreases. The broadening in eq 32 may be introduced via the σ_n^2 (eq 31) and/or the variation of the parameter C, which is a function of the individual homopolymer parameters B and T_0 (eqs 18b, 21, and 22). In this case, SI-60 in the investigated temperature range is in the weak segregation limit far from its ODT and, therefore, $S(\mathbf{q})$ is not affected strongly by the temperature variation. Thus, the broadening in Figure 8 is basically due to the influence of the VFTH parameters on C and to a lesser extent to the variation of the χ parameter with temperature. However, it is the presence of the composition fluctuations that discriminates between the block dynamics and leads to any excess broadening of the distribution. It should be noted here that the inherent widths in the relaxation spectra of the individual homopolymers, e.g., PI homopolymer, have not been introduced in the theoretical calculation up to this point. These will be introduced in the theoretical calculation of the dielectric loss spectra for the SI-60 diblock.

The dielectric loss that corresponds to the distribution of relaxation times of Figure 8 may be calculated using eq 12, which assumes a superposition of Debye distributions. However, in order to account for the natural width of the PI homopolymer distribution, a superposition of Cole–Davidson distributions is assumed, that has been found to describe PI homopolymer dielectric spectra (Figure 5 and ref 29). A similar assumption to account for the inherent distribution of the homopolymer has also been used when calculating the segmental dynamics in compatible homopolymer mixtures.[41] Therefore, eq 12 in the complex form becomes

$$\frac{\epsilon^*(\omega)}{\Delta\epsilon} = \int_{-\infty}^{\infty}\mu(\ln\tau)\frac{1}{[1 + i\omega\tau]^{\gamma_{CD}}}d(\ln\tau) \quad (40)$$

The theoretically calculated dielectric loss spectra for SI-60 using the $\mu(\ln\tau)$ distributions of Figure 8 and the convolution with the Cole–Davidson distribution (eq 40) are shown in Figure 9 for $\gamma_{CD} = 0.5$, close to the experimentally obtained value for homopolymers PI of molecular weight similar to the PI block of the copolymer.[42] The theoretical dielectric loss curves may now be compared

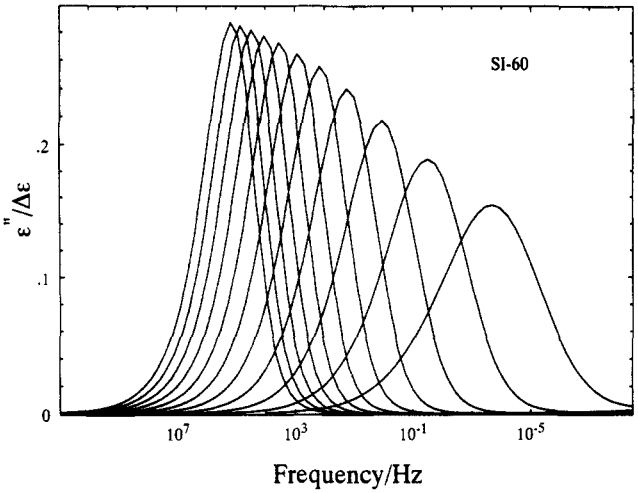

Figure 9. Calculated dielectric loss $\epsilon''(\omega)$ curves at various temperatures (from left to right, 365–265 K every 10 K) for SI-60 using the theoretical approach of section IV after convolution with the inherent distribution of homopolymer PI for $\gamma_{CD} = 0.5$.

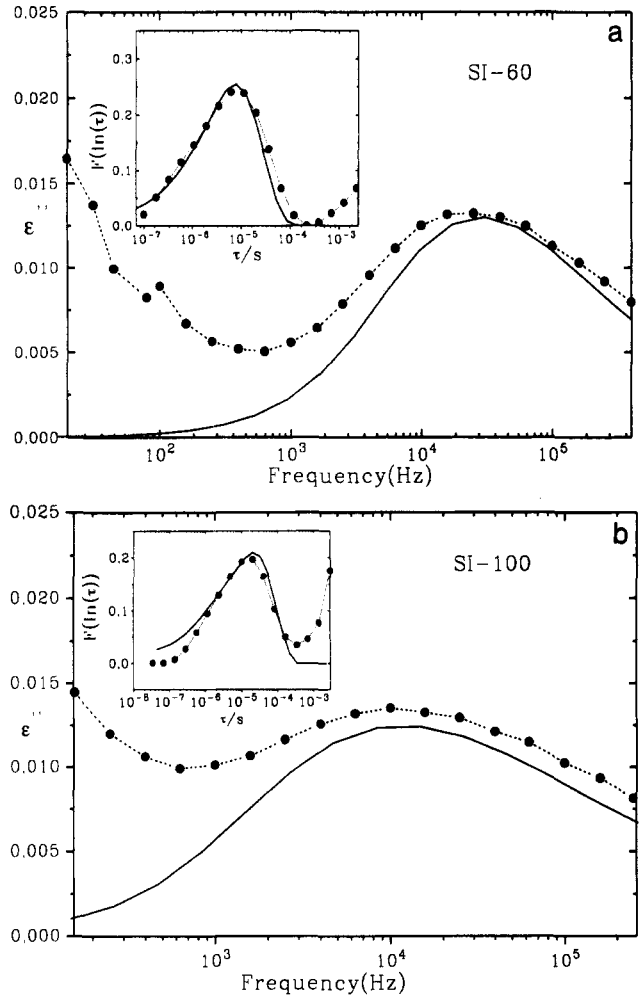

Figure 10. Comparison of the experimental dielectric loss data for (a) SI-60 at 345 K and (b) SI-100 at 355 K with the theoretically calculated curves with $\gamma_{CD} = 0.5$ and $\gamma_{CD} = 0.4$, respectively. In the insets the experimental distribution of relaxation times are compared to the ones obtained from the theoretical $\epsilon''(\omega)$ curves.

to the experimental data. The comparison for $\epsilon''(\omega)$ is shown in Figure 10 for (a) SI-60 at 345 K with $\gamma_{CD} = 0.5$ and (b) SI-100 at 355 K with $\gamma_{CD} = 0.4$. Note that the model does not consider the dc contribution that is present in the data at low frequencies. In fact, the tail of the dc contribution for, e.g., SI-60 at 345 K (see also Figure 3) extends to frequencies up to 10^4–10^5 Hz. It was deliberately avoided to add the empirical dc contribution to the model predictions and compare the results. Therefore, it is more appropriate to compare the distribution of relaxation times, obtained using the analysis of section III on the $\epsilon''(\omega)$ data, with the distribution of relaxation times obtained by CONTIN inversion of the theoretical dielectric loss spectrum, shown in the insets of parts a and b of Figure 10. The agreement for both diblock copolymers SI-60 and SI-100 of Figure 10 as well for the SI-110 diblock is very good. The semiadjustable parameter γ_{CD} varies similarly to its variation with molecular weight for homopolymer PI;[42] the parameter γ_{CD} was found to vary from 0.40 to 0.25 to 0.22 when the PI molecular weight increased from 11 000 to 41 900 to 102 000, whereas the theoretical value[40] based on either the Rouse or the tube models is 0.51, independent of molecular weight. The relaxation times and the widths of the distributions of relaxation times of the theoretical $\epsilon''(\omega)$ curves, shown in Figure 7, are in good agreement with the experimental data.

The broadening of the normal-mode distribution relaxation function $F(\ln \tau)$ of Figure 7b is the result of kinetic factors due to the proximity to the T_g and thermodynamic factors due to the proximity to the ODT. Both contributions are captured in eq 32; the kinetic factors via the parameter C (eq 21) and the thermodynamic factors via σ_n^2 that incorporates the structure factor $S(\mathbf{q})$ (eq 31). At high temperatures and equidistant from T_g, for example, at $T - T_g = 100$ K, samples SI-60 and SI-100 exhibit very similar $\Delta \ln \tau$, as both samples are also far from their ODT. As the temperature decreases, the effect of the composition fluctuations becomes important. For example, at $T - T_g = 75$ K, $F(\ln \tau)$ of SI-100 is about 25% broader than $F(\ln \tau)$ of SI-60 as is also evident from the different decreasing rates of $\Delta(\ln \tau)$ in Figure 7b. Consistently, the expected molecular weight dependence of the block relaxation times of SI-60 and SI-100 samples is observed at high temperatures, i.e., far from the T_g. Since block orientation is a large-scale motion, composition fluctuations have only a minor effect on the values of the normal-mode relaxation time,[25] compared to free volume effects determined by the average composition. Overall, these findings and considerations support the fact that the theoretical approach of this work can quantitatively account for the dielectric normal-mode relaxation in disordered diblock copolymer melts far from their ODT by taking into account effects of the proximity both to the T_g and to the ODT.

VI. Concluding Remarks

The normal-mode relaxation in symmetric disordered diblock copolymer melts far from the order-to-disorder transition, investigated using dielectric relaxation spectroscopy, was analyzed using a modification of the CONTIN routine, widely used in photon correlation spectroscopy, in order to quantitatively extract the distribution of relaxation times in the disordered diblocks. The widths of the normal-mode relaxation functions are significantly broader than the respective homopolymer distributions and show an extra broadening when the temperature is decreased and/or the molecular weight is increased. A theoretical approach is presented that considers composition fluctuation effects on the normal-mode relaxation. Both the short-range fluctuations due to chain connectivity, independent of the block/block interactions, and the long-range fluctuations in diblock copolymers due to the proximity to the ODT are coupled to the individual component segmental dynamics and result in broad distributions of relaxation times. When these are convoluted with the inherent homopolymer distributions due to higher modes, a quantitative agreement with the experimental dielectric loss spectra is obtained with only a semiadjustable parameter γ_{CD} that

varies with molecular weight similarly to the case of homopolymer polyisoprene.

In part 2[43] of this work, the normal-mode relaxation behavior for disordered diblock copolymers in the pretransitional regime near the ODT will be considered, where a bifurcation of the single dielectric normal-mode relaxation is observed by approaching the ODT. The low-frequency peak displays a temperature dependence similar to the temperature dependence of dielectric normal-mode relaxation far from the ODT, whereas the high-frequency component shows an apparent weak temperature dependence. These findings will be discussed in relation to computer simulations in disordered diblocks in the proximity to the ODT, where a similar splitting of the end-to-end orientation correlation function is observed.

Acknowledgment. A.N.S. acknowledges the hospitality and support of the Foundation for Research and Technology—Hellas. S.H.A. acknowledges that part of this research was sponsored by NATO's Scientific Affairs Division in the framework of the Science for Stability Programme and by the Greek General Secretariat of Research and Technology. G.F. and N.H. acknowledge partial support of the Greek General Secretariat of Research and Technology (Grant under the Operational Programme on Science and Technology). G.F. acknowledges partial support of the Alexander von Humboldt Foundation under Grant No. FOKOOP USS1685.

References and Notes

(1) Bates, F. S.; Fredrickson, G. H. *Annu. Rev. Phys. Chem.* **1990**, *41*, 525.
(2) Leibler, L. *Macromolecules* **1980**, *13*, 1602.
(3) Helfand, E.; Wasserman, Z. R. In *Developments in Block Copolymers—I*; Goodman, I., Ed.; Applied Science: London, 1982.
(4) Semenov, A. N. *Zh. Eksp. Teor. Fiz.* **1985**, *88*, 1242 (*Sov. Phys. JETP* **1985**, *61*, 733).
(5) Fredrickson, G. H.; Helfand, E. *J. Chem. Phys.* **1987**, *87*, 697. Barrat, G. L.; Fredrickson, G. H. *J. Chem. Phys.* **1991**, *95*, 1282.
(6) Bates, F. S.; Rosedale, J. H.; Fredrickson, G. H. *J. Chem. Phys.* **1990**, *92*, 6255. Rosedale, J. H.; Bates, F. S. *Macromolecules* **1990**, *23*, 2329.
(7) Fytas, G.; Anastasiadis, S. H. In *Disorder Effects on Relaxation Processes*; Richert, R., Blumen, A., Eds.; Springer-Verlag: Berlin, 1994.
(8) Quan, X.; Johnson, G. E.; Anderson, E. W.; Bates, F. S. *Macromolecules* **1989**, *22*, 2451.
(9) Adachi, K.; Nishi, I.; Doi, H.; Kotaka, T. *Macromolecules* **1991**, *24*, 5843.
(10) Yao, M.-L.; Watanabe, H.; Adachi, K.; Kotaka, T. *Macromolecules* **1991**, *24*, 2955.
(11) Yao, M.-L.; Watanabe, H.; Adachi, K.; Kotaka, T. *Macromolecules* **1991**, *24*, 6175.
(12) Kanetakis, J.; Fytas, G.; Kremer, F.; Pakula, T. *Macromolecules* **1992**, *25*, 3484.
(13) Alig, I.; Kremer, F.; Fytas, G.; Roovers, J. C. *Macromolecules* **1992**, *25*, 5277.
(14) Stühn, B.; Stickel, F. *Macromolecules* **1992**, *25*, 5306.
(15) Rizos, A.; Fytas, G.; Roovers, J. C. *J. Chem. Phys.* **1992**, *97*, 6925. Gerharz, B.; Vogt, S.; Fytas, G.; Fischer, E. W. *Prog. Colloid Polym. Sci.* **1993**, *91*, 58.
(16) Vogt, S.; Gerharz, B.; Fischer, E. W.; Fytas, G. *Macromolecules* **1992**, *25*, 5986.
(17) Anastasiadis, S. H.; Fytas, G.; Vogt, S.; Gerharz, B.; Fischer, E. W. *Europhys. Lett.* **1993**, *26*, 619.
(18) Jian, T.; Anastasiadis, S. H.; Fytas, G.; Adachi, K.; Kotaka, T. *Macromolecules* **1993**, *26*, 4706.
(19) Jian, T.; Semenov, A. N.; Anastasiadis, S. H.; Fytas, G.; Feh, F.-J.; Chu, B.; Vogt, S.; Wang, F.; Roovers, J. E. L. *J. Chem. Phys.* **1994**, *100*, 3286.
(20) Anastasiadis, S. H.; Fytas, G.; Vogt, S.; Fischer, E. W. *Phys. Rev. Lett.* **1993**, *70*, 2415. Fytas, G.; Anastasiadis, S. H.; Semenov, A. N. *Makromol. Chem., Macromol. Symp.* **1994**, *79*, 117.
(21) Vogt, S.; Anastasiadis, S. H.; Fytas, G.; Fischer, E. W. *Macromolecules*, in press.
(22) Vogt, S.; Jian, T.; Anastasiadis, S. H.; Fytas, G.; Fischer, E. W. *Macromolecules* **1993**, *26*, 3357.
(23) (a) Balsara, N. P.; Stepanek, P.; Lodge, T. P.; Tirrell, M. *Macromolecules* **1991**, *24*, 6227. (b) Balsara, N. P.; Eastman, C. E.; Foster, M. D.; Lodge, T. P.; Tirrell, M. *Makromol. Chem., Macromol. Symp.* **1991**, *45*, 213.
(24) Ehlich, D.; Takenaka, M.; Okamoto, S.; Hashimoto, T. *Macromolecules* **1993**, *26*, 189.
(25) Fytas, G.; Anastasiadis, S. H.; Karatasos, K.; Hadjichristidis, N. *Phys. Scr.* **1993**, *T49*, 237.
(26) Stockmayer, W. H. *Pure Appl. Chem.* **1967**, *15*, 539.
(27) Allen, V. R.; Fox, T. G. *J. Chem. Phys.* **1964**, *41*, 337.
(28) Cole, R. H. *J. Chem. Phys.* **1965**, *42*, 637.
(29) Bauer, M. E.; Stockmayer, W. H. *J. Chem. Phys.* **1965**, *43*, 4319. Adachi, K.; Kotaka, T. *Macromolecules* **1985**, *18*, 466. Boese, D.; Kremer, F. *Macromolecules* **1990**, *23*, 829.
(30) Adachi, K.; Kotaka, T. *Macromolecules* **1988**, *21*, 157. Adachi, K.; Kotaka, T. *Prog. Polym. Sci.* **1993**, *18*, 585.
(31) Havriliak, S.; Negami, S. *Polymer* **1967**, *8*, 161.
(32) Imanishi, Y.; Adachi, K.; Kotaka, T. *J. Chem. Phys.* **1988**, *89*, 7593.
(33) Liedermann, K.; Loidl, A. *J. Non-Cryst. Solids* **1993**, *155*, 26.
(34) Provencher, S. W. *Comput. Phys. Commun.* **1982**, *27*, 213; **1982**, *27*, 229.
(35) Fytas, G.; Meier, G. In *Dynamic Light Scattering*; Brown, W., Ed.; Oxford University Press: Oxford, U.K., 1993; Chapter 9, p 407.
(36) Alvarez Gonzalez, F. Ph.D. Dissertation, Universidad del Pais Vasco, 1993.
(37) Davidson, D. W. *Can. J. Chem.* **1961**, *39*, 571.
(38) Grossman, S. *Functionanalysis*; Aula-Verlag: Wiesbaden, Germany, 1988.
(39) Rouse, P. E. *J. Chem. Phys.* **1953**, *21*, 1272.
(40) Fujita, H. *Fortrschr. Hochpolym.-Forsch.* **1961**, *3*, 1.
(41) Fischer, E. W.; Zetsche, A. *Polym. Prepr. (Am. Chem. Soc., Div. Polym. Chem.)* **1992**, *33* (1), 78.
(42) Adachi, K.; Kotaka, T. *J. Mol. Fluids* **1987**, *36*, 75.
(43) Karatasos, K.; Anastasiadis, S. H.; Fytas, G.; Pispas, A.; Hadjichristidis, N.; Roovers, J. E. L.; Pakula, T. *Macromolecules*, in preparation.